A multiscale study of electronic structure and quantum transport in $C_{6n^2}H_{6n}$-based graphene quantum dots



2010 J. Phys.: Condens. Matter 22 095504

(http://iopscience.iop.org/0953-8984/22/9/095504)

J. Phys.: Condens. Matter **22** (2010) 095504 (11pp) doi:10.1088/0953-8984/22/9/095504

# A multiscale study of electronic structure and quantum transport in $C_{6n^2}H_{6n}$-based graphene quantum dots

**I Deretzis[1,2], G Forte[3], A Grassi[3], A La Magna[2], G Piccitto[4] and R Pucci[4]**

[1] Scuola Superiore, Università di Catania, I-95123 Catania, Italy
[2] CNR-IMM, I-95121 Catania, Italy
[3] Dipartimento di Scienze Chimiche, Università di Catania, I-95126 Catania, Italy
[4] Dipartimento di Fisica e Astronomia, Università di Catania, I-95123 Catania, Italy

E-mail: ioannis.deretzis@imm.cnr.it

Received 9 August 2009, in final form 16 December 2009
Published 15 February 2010
Online at stacks.iop.org/JPhysCM/22/095504

**Abstract**

We implement a bottom-up multiscale approach for the modeling of defect localization in $C_{6n^2}H_{6n}$ islands, i.e. graphene quantum dots with a hexagonal symmetry, by means of density functional and semiempirical approaches. Using the *ab initio* calculations as a reference, we recognize the theoretical framework under which semiempirical methods adequately describe the electronic structure of the studied systems and thereon proceed to the calculation of quantum transport within the nonequilibrium Green function formalism. The computational data reveal an impurity-like behavior of vacancies in these clusters and evidence the role of parameterization even within the same semiempirical context. In terms of conduction, failure to capture the proper chemical aspects in the presence of generic local alterations of the ideal atomic structure results in an improper description of the transport features. As an example, we show wavefunction localization phenomena induced by the presence of vacancies and discuss the importance of their modeling for the conduction characteristics of the studied structures.

(Some figures in this article are in colour only in the electronic version)

## 1. Introduction

Graphene is a carbon allotrope material that has triggered vast interest within both academic and industrial communities for its peculiar electrical, mechanical and optical characteristics [1]. Additionally, graphene is extremely convenient in terms of electronic structure modeling, since its planar monolayer topology and $sp^2$ hybridization allow for a simple and accurate $\pi$-orbital tight-binding (TB) description of its electronic bands [2, 3]. This approach has also been extensively implemented in the case of quantum transport studies of quasi-one-dimensional graphene constrictions with armchair or zigzag edges, widely known as graphene nanoribbons (GNRs) [4–7]. In the course of the last few years since graphene's laboratory isolation and due to the intense research on the field, experimental knowledge has grown; e.g. recent transmission electron microscopy images of monoatomic graphene flakes obtained with mechanical exfoliation have shown Stone–Wales defects and vacancies on the crystal membrane [8], while chemical reactivity with metal oxides has been achieved both in defected and in edge sites [9]. By means of first principles calculations, theory has demonstrated energetically favorable chemisorption processes on the areas that diverge from the perfect two-dimensional atomic lattice [10]. The aforementioned advances, among others, have raised new challenges in the field of graphene-based modeling in chemically and geometrically complex environments. Ideally, density functional theory (DFT) with appropriate exchange–correlation functionals could formulate an accurate and transferable framework for simulations on these systems [11, 12]. The undoubted intrinsic rigor of *ab initio* approaches is accompanied by computational overload limitations. In this sense, only the order of $\sim 10^3$ is affordable for all-electron bandstructure calculations (under

 

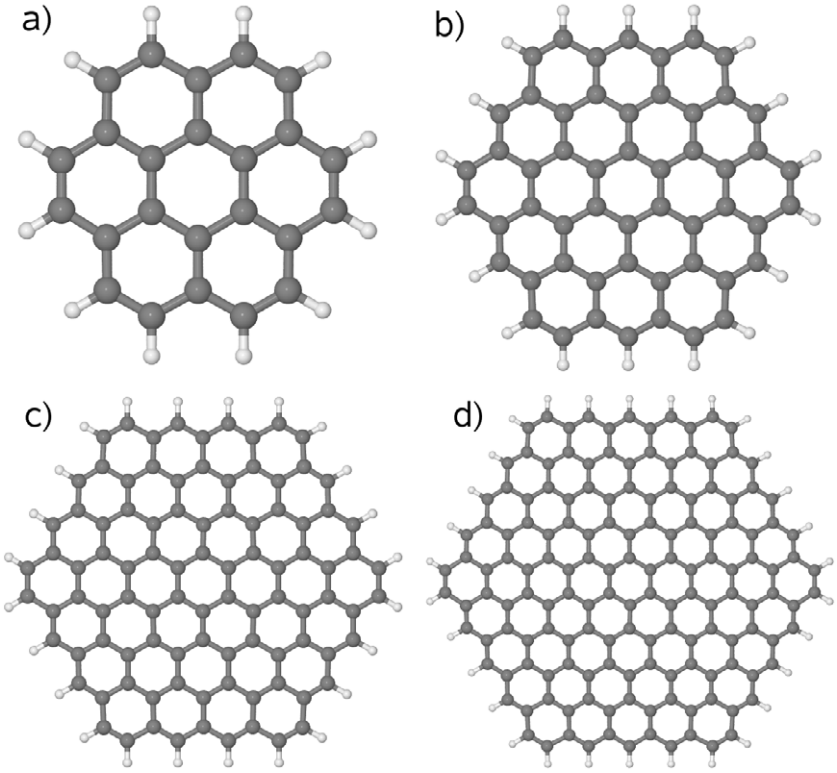


**Figure 1.** $C_{6n^2}H_{6n}$ molecular complexes: (a) $C_{24}H_{12}$ (coronene, $n = 2$), (b) $C_{54}H_{18}$ (coronene 19, $n = 3$), (c) $C_{96}H_{24}$ (coronene 37, $n = 4$), (d) $C_{150}H_{30}$ (coronene 61, $n = 5$).

linear scaling optimization techniques [13–16]), while an extra load has to be considered for self-consistent nonequilibrium quantum transport studies. Therefore, it becomes clear that a massive atomic reconstruction study in the presence of generic local alterations of the symmetry or the ideal atomic structure cannot be addressed with 'dogmatic' singular theoretical approaches (e.g. pure *ab initio* methods, pure TB studies etc), and a versatile multilevel approach would seem more appropriate.

In this paper a multiscale study of electronic structure and quantum transport is carried out for graphene quantum dot complexes. The study's groundwork focuses on: (i) the structural characteristics, and (ii) the methodological approach. The islands under consideration are the coronene molecules [17, 18], with a general chemical type of $C_{6n^2}H_{6n}$, in a pure, defected (with a single vacancy) and hydrogen functionalized form. These can be thought of as planar complexes of benzene rings that grow rotating around a central benzene ring, forming six hydrogen-passivated zigzag edges (see figure 1). Methodologically, the electronic structure is initially studied with DFT while the optical properties are calculated within time-dependent density functional theory (TD-DFT). These results serve as a reference for comparison with similar calculations by means of two parameterized semiempirical methods: (i) the extended Hückel (EH) theory [19] and (ii), the next-neighbor tight-binding model. Once a proper functional framework is identified for the semiempirical approaches the study proceeds with the calculation of electronic transport. Particular attention is paid to the effect of defect localization both within the level of characterization as well as model calibration, since the computational results indicate an impurity-like behavior of single vacancies in these systems. Conceptually, although the final objective is physical (quantum transport modeling in graphene islands), the basis is founded on chemistry (multiscale comparative analysis of the electronic structure).

The paper is organized as follows: in section 2 we review the methodological steps of the theoretical model, section 3 presents first principles and semiempirical electronic structure calculations for $C_{6n^2}H_{6n}$ islands up to $n = 5$, section 4 analyzes transport characteristics and focuses on the effects of local atomic reconstruction on the conductance, while in section 5 we discuss our results.

## 2. Methodology

Geometry relaxation and electronic structure properties (eigenvalues, eigenfunctions, density of states) of various $C_{6n^2}H_{6n}$ clusters are extrapolated by DFT calculations on a split-valence double-zeta (3-21g [20–22]) and a minimal (STO-3G [23, 24]) basis set, as implemented in the GAUSSIAN code [25]. The semiempirical three-parameter hybrid nonlocal exchange and correlation functional of Becke and Lee, Yang and Parr [26–29] (B3LYP) has been chosen here for its capacity to predict a large range of molecular properties for aromatic systems [30, 31]. Additional optical properties (excitation energies, fundamental optical gaps) are calculated within a TD-DFT approach for comparison between

theory and experiment. Electronic structure results are then compared with similar ones obtained by two semiempirical methods [32, 33] that also present a precision/efficiency mismatch among themselves: (i) the extended Hückel method, and (ii) a next-neighbor tight-binding model. In the case of the EH method three distinct parameterizations are used: (i) the first one considers a standard valence 2s2p-basis set of single-$\zeta$ Slater orbitals for C atoms, principally derived from the initial values used by Hoffmann [19] (EH-sp from now on)[5]. (ii) The second one is a 2s2p3d-based parameterization with valence/polarization double-$\zeta$ exponents and C parameters fitted to recreate the bandstructure of two-dimensional graphene as given by DFT calculations [34–36] (EH2-spd from now on). (iii) The third parameterization derives in a similar way to the second one, whereas here the polarization orbitals are absent [34, 35] (EH2-sp from now on). For the first-neighbor TB model a standard $t_0 = 2.7$ eV C–C hopping integral is used, while vacancies are approximated with the insertion of a local point potential $U \to \infty$ (unless explicitly referred to in the text). Although all methods construct the molecular orbitals on the basis of a linear combination of atomic orbitals, there is a distinct difference in the level of accuracy that each method delivers. In the DFT case the basis set is comprised of Gaussian-type orbitals with weighting coefficients that are both calculated self-consistently in order to reproduce the best approximation of the exact ground state density of the system. In the EH case the bases are nonorthogonal Slater-type orbitals with fixed weighting coefficients that have been parameterized on the basis of experimental data or first principles calculations. Finally in the TB case no real orbitals exist and the system Hamiltonian is constructed by a simple finite difference approach on next-neighbor atoms, which through a proper choice of the hopping integral is representative of the $\pi$-orbital in the $sp^2$ hybridization scheme. Naturally, the level of computational efficiency is the inverse, ranging from molecular (DFT) to mesoscopic (TB).

Electronic structure results are obtained through a direct diagonalization of the respective Hamiltonian matrix. Comparisons take place in terms of the highest occupied molecular orbital (HOMO) and the lowest unoccupied molecular orbital (LUMO) gaps, energy eigenstates $\epsilon_\alpha$ and their respective eigenfunctions $\Psi_\alpha$. The local density of states $\mathrm{LDOS}(\vec{r}, E)$ at the positions $\vec{r}$ of the device atoms at energy $E$ is calculated as

$$\mathrm{LDOS}(\vec{r}, E) = \sum_\alpha |\Psi_\alpha(\vec{r})|^2 \delta(E - \epsilon_\alpha), \qquad (1)$$

where $\delta$ is the Delta function, while summing over all atoms gives the total density of states (DOS) of the molecular systems at this energy.

Quantum transport is calculated within the nonequilibrium Green function formalism [37]. In particular, the method is based on the single particle retarded Green function matrix $G = [ES - H - \Sigma_\mathrm{L} - \Sigma_\mathrm{R}]^{-1}$, where $E$ is the energy, $H$ and $S$ are the device Hamiltonian and the overlap matrix respectively (written in an appropriate basis set), while $\Sigma_{\mathrm{L,R}}$ are the self-energy matrices that account for the effect of scattering due to the left (L) and right (R) contacts. In the TB case the overlap matrix coincides with the unitary one. The $\Sigma_{\mathrm{L,R}}$ terms can be expressed as $\Sigma = \tau g_\mathrm{s} \tau^\dagger$, where $g_\mathrm{s}$ is the surface Green function specific to the contact type and $\tau$ is the Hamiltonian relative to the interaction between the device and the contact. The calculation of the Green function permits for the evaluation of all the quantities of interest for conduction, e.g. the device spectral function is the anti-Hermitian part of the Green function $A = \imath(G - G^\dagger)$, from which the density of states can be obtained as $D(E) = \frac{1}{2\pi}\mathrm{Trace}(AS)$. Moreover, in the coherent transport regime, the expression used for the zero-bias transmission probability reads $T(E) = \mathrm{Trace}(\Gamma_\mathrm{L} G \Gamma_\mathrm{R} G^\dagger)$, where $\Gamma_{\mathrm{L,R}} = \imath(\Sigma_{\mathrm{L,R}} - \Sigma_{\mathrm{L,R}}^\dagger)$ are the contact spectral functions.

In this study $C_{24}H_{12}$, $C_{54}H_{18}$, $C_{96}H_{24}$ and $C_{150}H_{30}$ complexes have been considered in their pure, defected (with a single vacancy) and hydrogen functionalized form. All structures have been relaxed by DFT molecular dynamics while relaxation information is also used by the EH method. In the case of TB an ideal reconstruction of the molecular structure is considered, since the latter does not account for interatomic distances. Finally, for the quantum transport calculations the islands are placed within two semi-infinite Au(111) metallic planes (directly considered in the case of EH, appropriately fitted in the case of TB [33]) in a molecular bridge configuration.

## 3. Comparative analysis of the electronic structure between first principles and semiempirical methods

A proper treatment of quantum transport modeling has to take account of both quantitative and qualitative aspects of the electronic structure of a molecular system. In this sense, if the value of the HOMO–LUMO gap is a quantitative feature, the form of the HOMO and LUMO wavefunctions, or similarly, the local density of states of the structure for energies near the HOMO/LUMO states, are qualitative characteristics. It can be argued that in terms of conduction, although the former can influence scaling, the latter can affect the shape of the current–voltage curve. In addition, higher-bias conduction requires accuracy for the entire conduction/valence bands. Such considerations imply that a proper description of the local density of states of a molecular system by means of a quantum chemical method can be fundamental for correct modeling in terms of quantum transport. This section examines electronic configuration aspects one by one.

### *3.1. Geometry relaxation*

From a numerical point of view, the distance between the atomic sites influences the electronic structure of a molecular system by affecting both overlap and Hamiltonian matrix elements. Geometry relaxation with the DFT method has shown that, near the island edges, complex distance polymerization effects can be observed that tend to periodically

[5] $\mathrm{Eon-site(C_s)} = -21.4$ eV, $\mathrm{Eon-site(C_p)} = -11.4$ eV, $\mathrm{Eon-site(H)} = -13.6$ eV, $\zeta(\mathrm{C_s}) = 1.625$, $\zeta(\mathrm{C_p}) = 1.625$, $\zeta(H) = 1.3$, $\mathrm{coeff(C_s)} = 1$, $\mathrm{coeff(C_p)} = 1$, $\mathrm{coeff(H)} = 1$, $K = 1.75$.

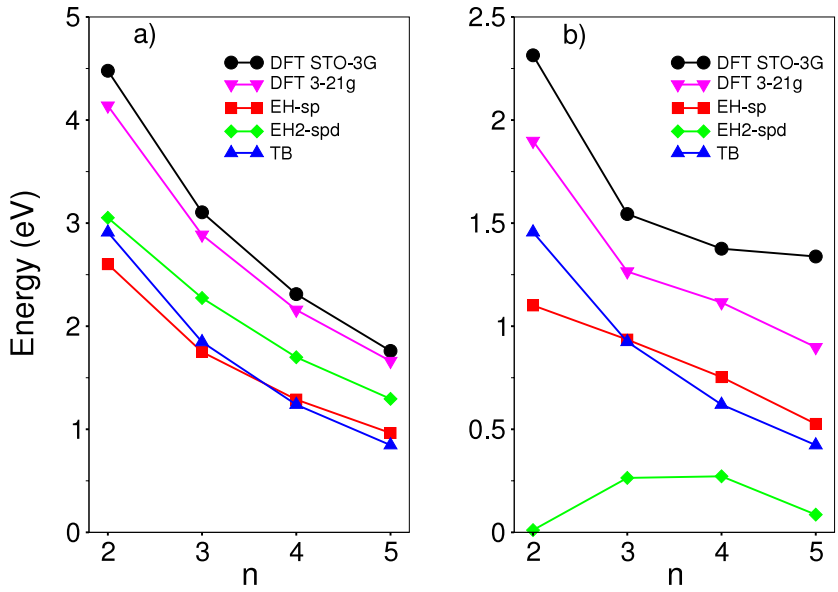


**Figure 2.** HOMO–LUMO gaps of pure (a) and defected (b) $C_{6n^2}H_{6n}$ quantum dots by means of DFT, EH and TB.

increase/decrease C–C bonding by about 5% from the equilibrium distance (C–$C_{\text{equil}} \approx 1.42$ Å). Such a feature also tends to propagate in the inner parts of the clusters, albeit in a continuously decreasing extent, while only the central benzene rings result in having equal interatomic C distances. Distance shortening due to hydrogen passivation has also been observed in the case of graphene nanoribbons [11], whereas the effect there is localized near the edges. From a methodological point of view, variable bond-lengths can have a practical consequence in the parameterization of the hopping integral for the TB method, where for accuracy's sake an evaluation of each atomic pair distance should take place prior to the assignment of the integral value (in this sense the method becomes similar to the single $\pi$-orbital Hückel one). If such information is not available inaccuracies in the TB Hamiltonian can occur. It can be argued that further complications in the correct estimation of interatomic distances have to be considered in the case of the interaction between the molecular structures and a substrate (e.g. for the reproduction of laboratory conditions [38–40]). In this case combined molecular/substrate atomistic modeling should include interface bonding interactions for both the chemical and the structural characteristics.

### *3.2. Energy levels*

A well-known aspect of geometrical symmetry is the presence of orbital degeneracies. Such a feature is captured by all the methods for the pure structures, from DFT to TB. Eventually, symmetry breaking events (e.g. the presence of a single vacancy) lift such degeneracies and split the respective energy levels. In this subsection we visualize the characteristics of the eigenvalue spectrum in a full quantum scale, in terms of energy gaps and state alignment over the energy axis. Figure 2 shows HOMO–LUMO gaps for pure and defected structures by means of DFT (both 3-21g and STO-3G), EH2-spd, EH-sp and TB, while EH2-sp results are similar to EH2-spd and are not shown. Regarding the pure structures, the following observations can be made: (i) the gap value given by DFT is larger than those obtained by the semiempirical methods. This aspect is not directly related to the exchange–correlation absence in the semiempirical cases (since parameterization can take place on the basis of *ab initio* calculations) but to the chemical environment considered for the parameterization, which usually considers bulk structures where the effect of confinement cannot be evaluated. Moreover, it is interesting to see that the minimal basis set in the DFT method slightly overestimates this value with respect to the 3-21g case. (ii) The EH2-spd method, with its orbital foundation and $sp^2$-hybridized calibration, better approximates the DFT results with respect to the other semiempirical methods. (iii) Albeit the clear difference in terms of the methodology, results by EH-sp and TB are very similar. It should be noted here, that a rough method to bring semiempirical models closer to first principles calculations is by globally fitting the hopping integral (or similarly the Wolfsberg–Helmholtz $K$ constant for EH). However in this case the parameterization loses any meaning outside the designated geometrical environment.

The validity of the results obtained by the first principles B3LYP/32-1g model for these structures with respect to the semiempirical methods is tested by direct comparison with experimental data on the fundamental optical gap of the $C_{24}H_{12}$ island. For this purpose we follow a TD-DFT approach for the calculation of the excitation energies of this cluster. The calculated value for the fundamental optical gap is $E_{\text{opt}} = 3.18$ eV, which is in a good agreement with the experimental value of $E_{\text{opt}} = 3.29$ eV measured in [38][6]. The difference between the ground state ($E_{\text{HOMO–LUMO}} = 4.13$ eV) and

[6] We have confirmed the good TD-DFT estimation of the optical gap with respect to the experimental value by also calculating excited state energies within the configuration interaction singles (CIS) method. The optical gap given by the latter is $E_{\text{opt}} = 4.19$ eV, which is by far bigger than the experimental and the TD-DFT value.

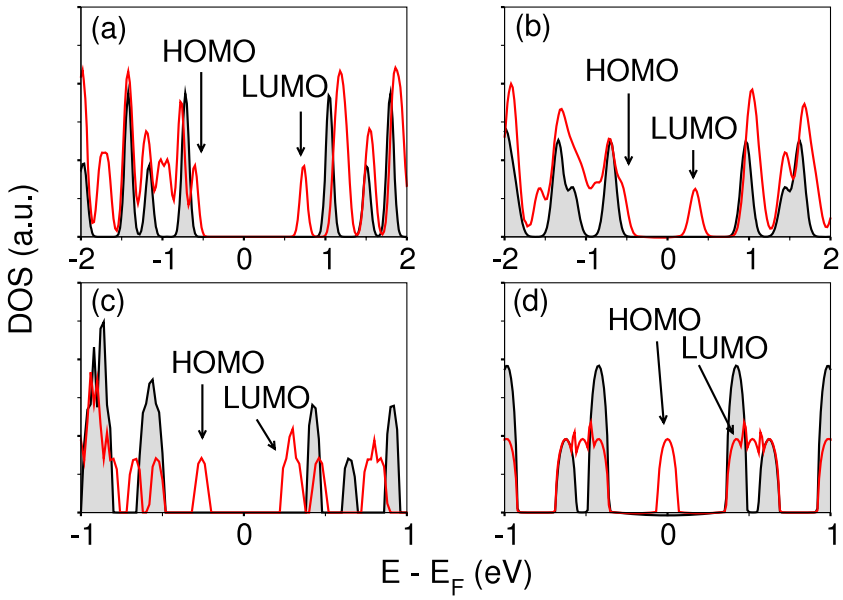


**Figure 3.** Density of states around the Fermi level for pure (filled line) and defected (unfilled line) $n = 5$ islands by means of (a) DFT (STO-3G), (b) DFT (3-21g) (c) EH-sp and (d) TB. In all cases, a small smearing has been applied.

the excited state ($E_{\text{opt}} = 3.18$ eV) is also consistent with experimental measurements for similar structures, since the exciton binding energy in these complexes gives rise to a 0.5–1 eV reduction of the optical gap with respect to the ground state HOMO–LUMO gap [41].

Moving on to the defected structures (with a single vacancy in the central benzene ring) an expected reduction of the gap value can be observed, while DFT basis set differences become more pronounced. For the semiempirical methods the picture changes qualitatively only in the EH2-spd case. Considering spin-degeneracy, the EH2-spd parameterization assigns the HOMO and the LUMO states to two quasi-degenerate levels prior to the real gap, which in this case is represented by the LUMO and LUMO + 1. A detailed study of the corresponding eigenvectors (with respect to eigenvectors given by the DFT and EH-sp) shows that in the case of the defected structures an incorrect state is inserted at the energy axis inside the energy gap. In this sense, although the EH2-spd/EH2-sp parameterizations demonstrate overall optimal characteristics (e.g. see [35] for a study on carbon nanotube bandstructure and the next subsection for pure clusters), a careful use might be necessary for transport calculations in defected coronene systems.

Another important aspect that concerns energy eigenstates is their alignment over the energy axis, especially when local alterations of the symmetry 'break' the ideal atomic structure. For few-atom molecular complexes, a neat way to visualize this is with their density of states spectrum as a function of energy. Figure 3 plots DOS functions for pure and defected $n = 5$ islands by means of DFT, EH-sp and TB. In this case the lifting of the symmetry-induced degeneracy inserts states that tend to 'shrink' the band gap. In the case of TB, a state always appears in the center of the pure structure's gap. This well-known effect has its origin in the bipartite nature of the honeycomb lattice, where the presence of a single vacancy in one of the two sublattices inserts a zero-energy mode at the Fermi level of the system (i.e. at energy $E = 0$) [42]. The key issue arising from figure 3 is that for the more sophisticated methods the HOMO state is not located in the center of the pure structure's gap, but shifted towards lower energies next to the valence band. Such a feature is captured by both DFT and EH-sp, although in quantitative disagreement. The analysis therefore implies that TB gives a rigid picture of the gap state with respect to more sophisticated models. With this perspective, this study will try to confront the problem by introducing a further parameterization for the point defect (see section 4).

### *3.3. Qualitative evaluation: molecular orbitals*

The most important aspect for transport in nanostructures is the availability of states (either full or empty) within the conduction window. In conjunction, a very important factor for the correct treatment of conduction are the eigenvectors that correspond to these states, from which topological features can be deduced (e.g. localization, polarization etc). In this context the semiempirical methods have been evaluated on the basis of DFT results for pure, defected and hydrogen functionalized structures. Results shown here are for the DFT 3-21g, EH-sp, EH2-sp and TB models. A qualitative correspondence has been obtained for the DFT STO-3G and the EH2-spd bases with respect to their method counterparts[7].

*3.3.1. Pure structures.* TB: in the absence of real atomic orbitals and with the restriction of its limited basis set the TB method demonstrates a progressive wavefunction descriptive capacity from smaller to larger complexes. In particular, TB

[7] The surprisingly accurate correspondence in terms of molecular orbitals obtained for the 3-21g and STO-3G bases within the DFT scheme indicates that the minimal basis set can be used in disordered graphene-based systems with only small quantitative compromises (see section 3.2).

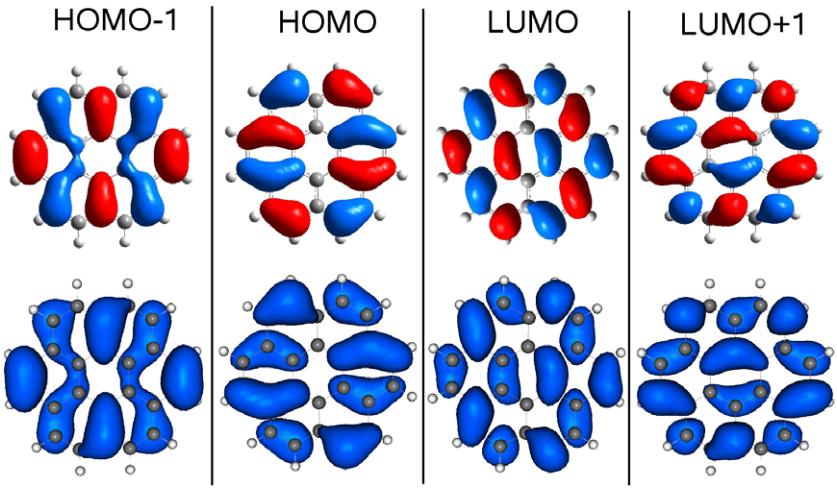


**Figure 4.** Molecular orbitals for the HOMO-1, HOMO, LUMO and LUMO + 1 states of the $n = 2$ complex by means of DFT (upper) and EH-sp (lower).

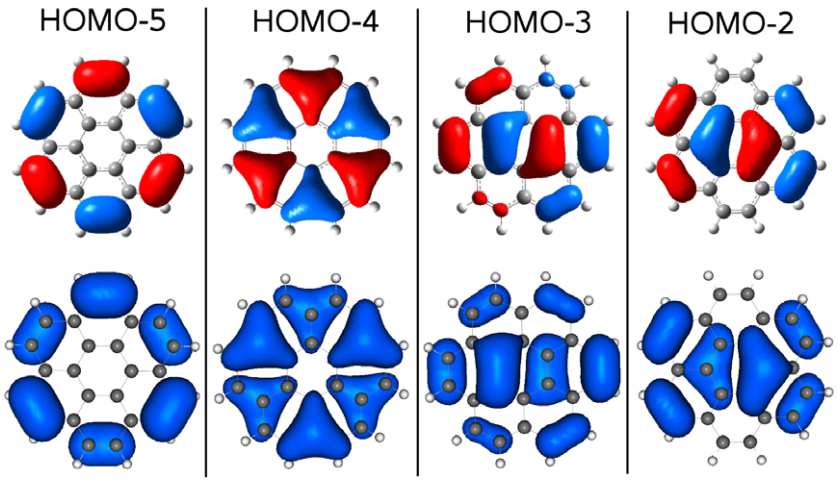


**Figure 5.** Molecular orbitals for the HOMO-5, HOMO-4, HOMO-3 and HOMO-2 states of the $n = 2$ complex by means of DFT (upper) and EH2-sp (lower).

eigenvectors for conduction/valence eigenstates bear a poor resemblance with the respective DFT ones for the $C_{24}H_{12}$ molecule, while the similarity becomes gradually better for larger structures. This behavior is due to the C–C bonding distance polymerization features discussed earlier, which have a higher impact for the smaller complexes. Arriving at the $n = 5$ complex, DFT-TB matching becomes adequate, hence, the TB method is qualified for the electronic structure description of these structures with a respective number of C atoms and onwards.

EH-sp: the method is in a qualitative agreement with the DFT one only for the energy degenerate HOMO/HOMO − 1 and LUMO/LUMO + 1 pairs for all studied structures (see figure 4 for the coronene molecule). Moving away from these states towards the valence band, accuracy is lost, not in the form of the wavefunctions but in the correct order that these appear. Conduction band description results are poor.

EH2-sp: matching between EH2-sp and DFT wavefunctions is excellent for all pure islands and for both valence and conduction energy zones (e.g. see figure 5 for the valence band of $C_{24}H_{12}$). Here it is evident that the chemical environment in which the parameterization has taken place (bulk graphene) and the double-exponent Slater orbitals play a crucial role in the representation of the correct molecular orbitals. It is also interesting to note the mismatch in the results obtained by the EH2-sp and the EH-sp parameterizations, even if the quantum chemical method is the same.

Finally, magnetism issues that could arise due to the presence of zigzag terminated edges in these complexes are not confirmed by the *ab initio* calculations, contrary to zigzag GNRs [11, 12, 43] or coronene islands above a critical size (based on mean-field Hubbard model calculations [44]). It can therefore be stated that the absence of a self-consistent exchange evaluation in the semiempirical methods does not compromise the obtained results with respect to the DFT case in the present study.

*3.3.2. Defected structures.* The presence of a single vacancy in these islands provokes a distortion of the atomic structure, since the remaining $\sigma$ dangling bonds tend to recombine by

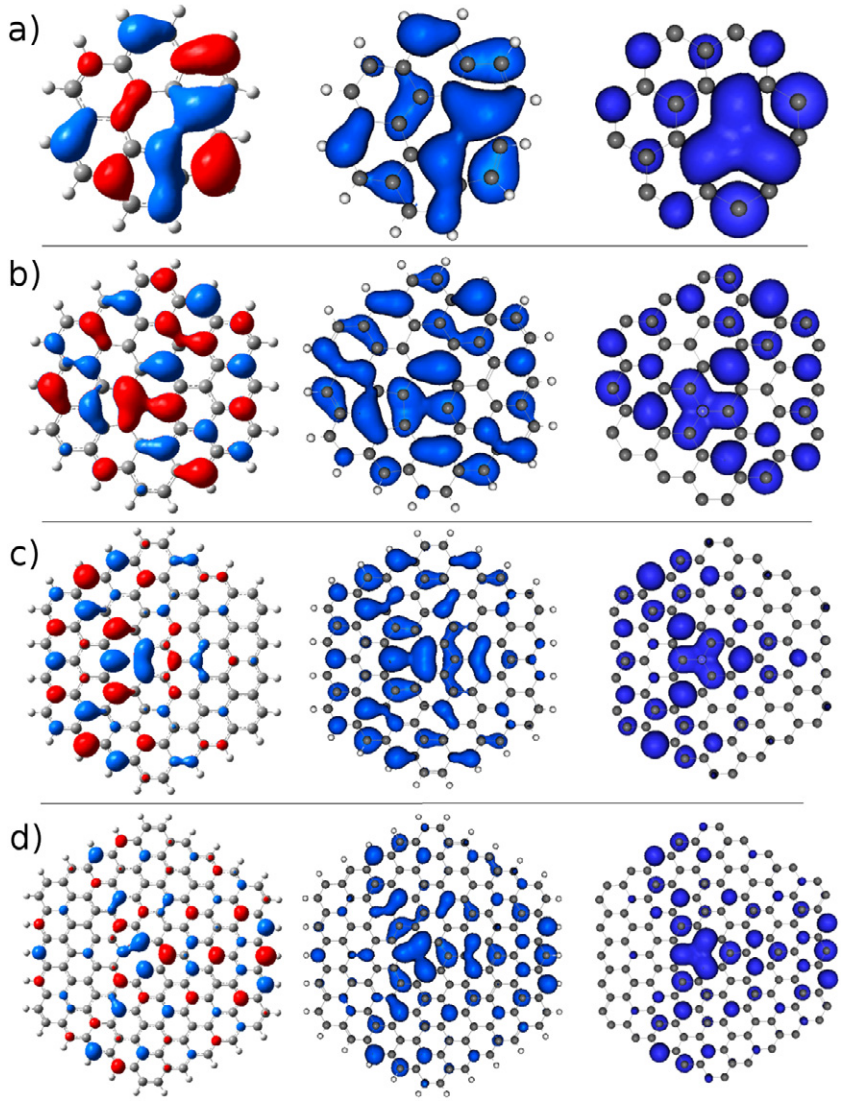


**Figure 6.** Highest occupied molecular orbitals for (a) $n = 2$, (b) $n = 3$, (c) $n = 4$ and (d) $n = 5$ islands with a single vacancy by means of DFT (left), EH-sp (middle) and TB (right). The TB orbital representation is demonstrated by assigning Slater-type $p_z$-orbitals with the same parameters as the EH method.

leaving their equilibrium positions. On the other hand, $\sigma$-orbital energies are too far away from the HOMO–LUMO states and do not contribute to the formulation of the respective wavefunctions. Most importantly, apart from a symmetry breaking effect in topological terms, the presence of the vacancy imposes a localization of the wavefunctions that correspond to the various eigenstates, making such complexes 'sensitive' to the positioning of a nanoprobe. In terms of the various methodologies we have obtained:

TB: the lack of information concerning distance in the TB method is even more important for the defected structures, where the smaller the structure the higher is the effect of the vacancy on its deformation. In this sense the TB method, with its standard parameterization, is inadequate for the description of the electronic structure of these complexes, whereas as in the case of pure structures, description gradually betters as the complexes grow, with the following particularities: (i) HOMO wavevectors present a succession of zero and non-zero values for neighboring atomic sites and (ii) for even $n$-indexed molecules ($n = 3, 5$ etc) the hexagonal edge that corresponds to the defected site presents atoms with zero LDOS for the HOMO eigenstate (figure 6). This last observation is crucial in terms of transport modeling, and its implications will be discussed in section 4.

EH-sp: it describes better the valence (HOMO, HOMO-1, HOMO-2) than the conduction band. Moreover, moving towards larger structures the accuracy is increased and for the $n = 5$ island description becomes adequate for the valence and discrete for the conduction band.

EH2-sp: the main drawback of this parameterization concerns the presence of an incorrect HOMO eigenstate as discussed in section 3.2. Overall it offers a valid alternative to the DFT results, on the other hand, though, the importance of the HOMO state in terms of conduction modeling requires attention in its use in defected graphene environments.

Finally a remark on the $C_3$ point symmetry of the HOMO wavefunction around the vacancy should be made [42] (a feature that is captured by all methods), where clearly a

non-zero magnetic moment arises (also obtained with Hartree–Fock-based calculations on the same complexes [18]).

*3.3.3. Hydrogen functionalized structures.* Results for the complexes where the defected site has been functionalized by a hydrogen atom that saturates one $\sigma$ dangling bond do not differ substantially from their nonfunctionalized counterparts. Here the role of hydrogen slightly influences the structure's geometrical relaxation, whereas wavefunctions are similar to non-passivated molecules with defects, as $\sigma$-orbital energies are too far away from the zone of interest for conduction. Consequently, the discussion made in the previous subsection is also valid in this case for methods that directly account for the presence of hydrogen (DFT, EH).

### *3.4. Conclusion*

Semiempirical models in graphene-based quantum dot structures can be successfully used within a certain framework that is established by their quantum chemical limitations. The Extended Hückel method, with its real-orbital foundation, can cope with a great number of qualitative features, whereas the role of parameterization proves to be fundamental. In this sense EH2-spd/EH2-sp are excellent alternatives to DFT for pure coronene structures, whereas defected/functionalized complexes are more appropriately treated by the EH-sp model. On the other hand, TB with the standard parameterization can be used for the study of conduction in large defect-free systems, while modeling remains a challenge for defected complexes since results appear too 'radical'. In this sense a further parameterization of the defected site within its particular topological environment is necessary for the correct estimation of the electronic structure, an argument that will be treated in section 4.

## 4. Quantum transport

The study's bottom line is to efficiently model transport phenomena on graphene-based quantum dot systems respecting the chemical aspects that arise due to the particularity of the chemical/geometrical environment. The importance of a proper description of the electronic structure on conduction can be better appreciated in the case of defected islands, where the presence of the vacancy is also a reason for topological asymmetries on the formation of the molecular orbitals (see figure 6). In this section, a numerical analysis takes place for the defected $n = 5$ complex, initially with the EH-sp method, while results are used for a critical evaluation of similar calculations made with the TB model. Two equivalent molecular bridge configurations are used, where the source-device-drain geometry differs only in the position of the contacts with respect to the vacancy site (figure 7). In detail, two opposite edge corners of the aforementioned dot have been inserted between two semi-infinite Au(111) metallic planes, which model the metallic probes of an atomic force microscope. The contact Hamiltonian is also written within the EH theory using an appropriate spd basis [33]. A prerequisite of equivalence for the contact bonding between the two configurations is explicitly requested

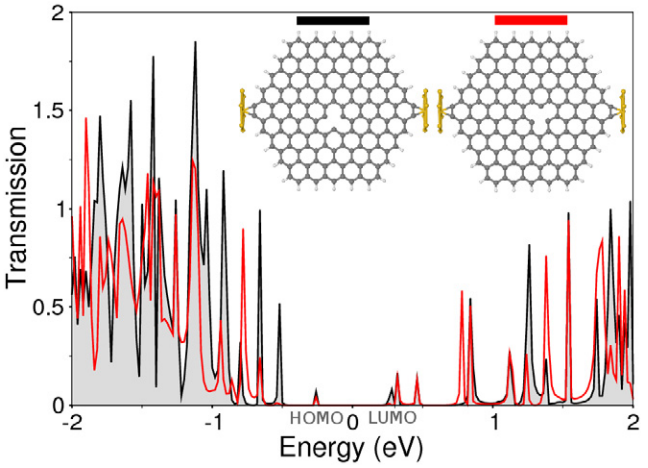


**Figure 7.** Transmission as a function of energy, by means of EH-sp for the defected $n = 5$ complex, for two equivalent contact configurations that differ only in the position with respect to the defected site.

for an evaluation of transport without geometrical or bond strength implications [33]. Here, contacts are 1.7 Å distant from the edge C atoms (avoiding strong invasiveness) and are geometrically symmetrical with respect to the molecular structure. The transmission probabilities obtained for the two configurations have a distinct character, whereas differences are not fundamental for the conduction characterization of the system. Namely, both configurations give a non-zero transmission value corresponding to the HOMO state, whereas differences exist both in the valence and conduction band. The divergences can only be attributed to the different geometrical positions of the contacts with respect to vacancies that reflect unequal interface chemical bondings due to orbital localization phenomena. The minor impact of such phenomena on the conduction characteristics is driven by the real atomic orbital foundation of both contact and device wavefunctions that constitute bonding interactions that exceed next-neighbor distances. Therefore, e.g. if local disorder provokes a nullification of the LDOS at the contact–device interface at a certain energy, transmission is still possible if this zero LDOS expands in a smaller area than that of orbital overlap between the contact and further device atoms with a finite LDOS. The same concept can be described from a quantum mechanical perspective, where the presence of the contacts induces a constant perturbation on the bare device's Hamiltonian and the effective Hamiltonian now is written as

$$\hat{H}_{\mathrm{eff}} = \hat{H}_0 + \hat{H}_{0\mathrm{L}} + \hat{H}_{0\mathrm{R}}. \tag{2}$$

Here $\hat{H}_0$ corresponds to the molecular Hamiltonian in the absence of the contacts and $\hat{H}_{0\mathrm{L},0\mathrm{R}}$ are the Hamiltonian components that arise due to the interaction between the device and the left/right contact. According to EH theory, for the localized HOMO state we get

$$\langle \Psi_{\mathrm{HOMO}} | \hat{H}_{0\mathrm{L}} | \Psi_{\mathrm{HOMO}} \rangle \neq 0 \tag{3}$$

and

$$\langle \Psi_{\mathrm{HOMO}} | \hat{H}_{0\mathrm{R}} | \Psi_{\mathrm{HOMO}} \rangle \neq 0. \tag{4}$$

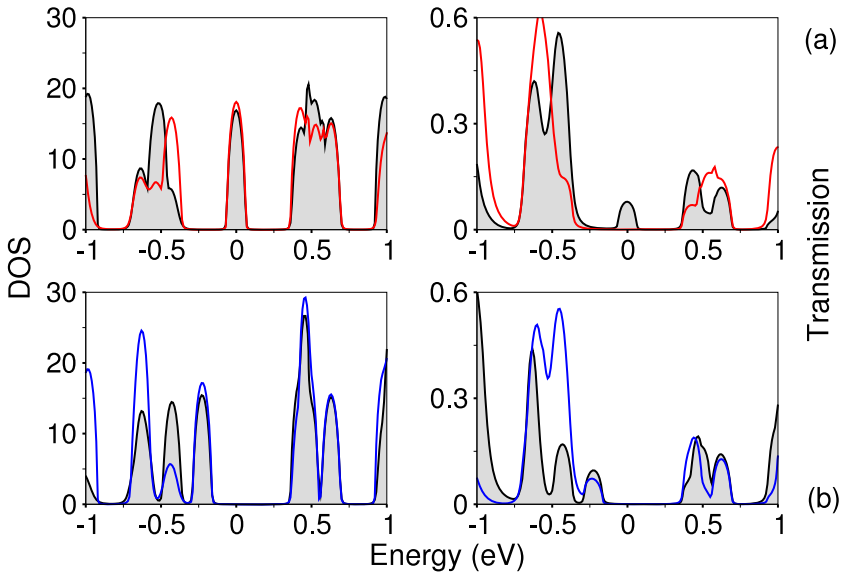


**Figure 8.** Density of states and transmission probability of the $n = 5$ complex by means of the TB method for nonparameterized (a) and parameterized (b) vacancy values (Eon $-$ site$_{vac} = 10$ eV, $t_0 = 1.9$ eV). The DOS figures are represented with a small Gaussian smearing.

This finite value of both integrals makes transport plausible from the HOMO state.

Albeit its phenomenological simplicity, the TB description of conduction in the same structures as before generates complexity in the interpretation of the obtained results. There are two critical points: (i) the first has to do with the zero mode introduced by the vacancy at the Fermi energy level. The corresponding HOMO wavefunction, and equally the LDOS at $E = 0$, have a succession of finite and zero values for next-neighbor atoms, that is, for each C atom with a finite LDOS value the three nearest-neighbor atoms have a zero value and vice versa. Moreover, the $n = 5$ structure (like all even $n$-indexed ones) has a hexagonal side with LDOS $= 0$, as discussed in the previous section. Therefore, for the standard-parameterized first-neighbor TB model this state represents the respective molecular orbital in a rigid way, contrary to EH and DFT. (ii) The second issue reflects TB interface bonding issues between a device and the metallic leads that in the next-neighbor context present a strongly-localized character (e.g. only two C atoms in our case are allowed to chemically interact with the leads). In this case, if the metallic contacts form bonding interactions exclusively with zero LDOS carbon atoms (configuration two in our case), the HOMO eigenstate will not contribute to the conductivity of the system, yielding a zero transmission probability at that energy. Indeed, figure 8 shows the transmission, as a function of energy, for the $n = 5$ complex for the two contact configurations presented before, where a finite transmission probability for the HOMO state appears only in the first case, whereas clearly no conduction takes place through this state for the second. In terms of expectation values, for the HOMO eigenstate of the second configuration we now get

$$\langle \Psi_{\mathrm{HOMO}} | \hat{H}_{0\mathrm{R}} | \Psi_{\mathrm{HOMO}} \rangle = 0. \tag{5}$$

This blocked conduction channel reflects the extreme manifestation of wavefunction localization obtained by TB and contrasts with the EH results. It is therefore fundamental that realistic modeling has to take into account that the tails of the contact wavefunctions penetrate the body of a molecular device for several Å before they decay.

A possible way to confront the aforementioned problems is by introducing a further parameterization of the vacancy site. Figure 9 shows a schematic LDOS real-space representation of the $n = 5$ island by means of the TB method for a nonparameterized and a parameterized vacancy site. The vacancy parameterization takes place by assigning a finite $E = 10$ eV energy to the site and a $t_0 = 1.9$ eV hopping integral within this and the neighboring atoms. The principal differentiations obtained are: (i) the sites where zero LDOS values corresponded for the HOMO level now obtain a finite, albeit small density (not visible in figure 9). (ii) The hexagonal edge that corresponds to the vacant site (which for even $n$-indexed molecules had zero HOMO wavefunction components) also obtains a finite LDOS value that is more similar to the electronic structure by means of the DFT and the EH methods (see figure 6). (iii) The collocation of the HOMO eigenstate on the energy axis is in $E < 0$, i.e. it moves towards the valance band, leaving the midgap position (see figure 8). Also, in this case, the DOS spectrum comes closer to the ones obtained by DFT and EH (figure 3). Finally, changes obtained for wavefunctions that correspond to other than the HOMO level do not present particular differences from their nonparameterized counterparts. Overall, the parameterization of the vacancy site permits a clear improvement of the qualitative aspects of the electronic structure for defected molecules, respecting the chemical equilibrium and approaching the results obtained by more sophisticated methods. Indeed, in terms of transport, the HOMO eigenstate now contributes to conduction for both contact configurations, whereas a less 'radical' representation of the transmission probability is sketched. Apart from the qualitative gains of TB calibration presented here, a key

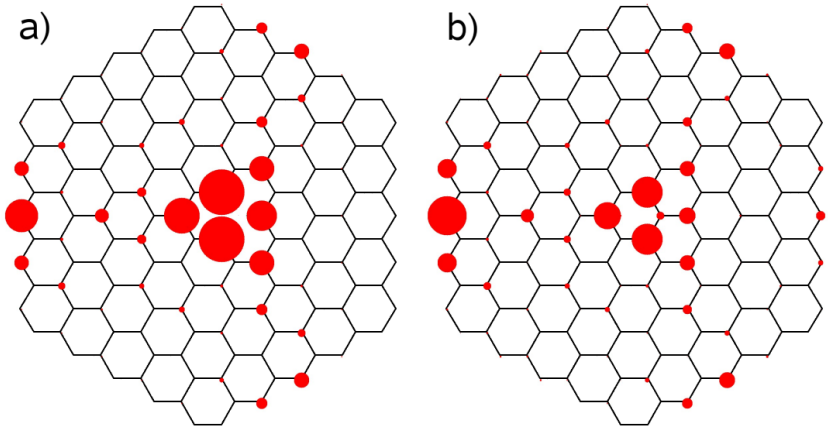


**Figure 9.** Schematic LDOS representation of the $n = 5$ complex by means of the TB model for two different parameterizations of the vacancy site, (a) $t_0 = 0$ eV within the vacancy and the neighboring sites, and (b) $t_0 = 1.9$ eV and Eon $-$ site$_{vac} = 10$ eV. The radius of each circle is proportional to the amplitude of the LDOS value on that atomic site.

conceptual issue arises. Now the vacancy site becomes similar to a (nominally p-type) impurity, since the local point potential drops (from $\infty$ to big finite) and the hopping integral rises (from 0 eV to finite) [42]. This consideration can have an impact on the way vacancies are seen in graphene-based systems, both from an application as well as from a methodological point of view. As a conclusion, it should be strongly stated that the common perception of treating vacancies in graphene-based systems (zero-energy modes) is not confirmed in this study; an impurity-like behavior has been obtained.

## 5. Discussion

One important aspect of the understanding of impurity induced disorder in graphene is the possibility of controllable band gap tailoring for semiconductor applications [45, 46]. This study evidences that vacancies in graphene complexes actually behave as impurities. Such a consideration can have a big practical impact on the engineering of mobility gaps in graphene-based systems, since vacancies are easier to obtain (e.g. by ion irradiation [47]) than actual p- or n-type doping. Here we have attempted to confront modeling issues for pure and defected graphene quantum dot islands, keeping in mind that the desired computational efficiency for the simulation of large systems should not be in contrast with chemical accuracy. In this sense a multiscale approach has been introduced with the scope to identify the merits and limitations of semiempirical approaches within a designated chemical environment prior to their use for the calculation of quantum transport. Model confrontations have demonstrated that no perfect matching exists between the results obtained by the *ab initio* approach on the one hand and the semiempirical approaches on the other. The extended Hückel method, with its real-orbital foundation, manages to capture a wide set of qualitative aspects of the systems, which qualify it as an appropriate method for quantum transport calculations in graphene-based environments. Moving towards computational efficiency, the tight-binding model has confirmed its authoritativeness for pure large-scale structures, whereas when structural defects have to be taken into account a further parameterization of these sites needs to be considered. It is unlikely that such tuning can be generic for all types of complexes/defect-types, since the influence of the chemical environment can be fundamental. For example, we have to note that by only adding a second vacancy in the vicinity of the same triangular sublattice of the honeycomb structure, hybridization between the two modes can take place. In this sense, a model evaluation of TB by a more sophisticated method should ideally take place prior to its use in disordered graphene-based systems. It should be finally pointed out that both theoretical and experimental attention should be paid to strongly defected systems where topological disorder can be a reason for wavefunction localizations, whose influence on the electronic properties could be important.

## References

[1] Geim A K and Novoselov K S 2007 The rise of graphene *Nat. Mater.* **6** 183–91
[2] Wallace P R 1947 The band theory of graphite *Phys. Rev.* **71** 622–34
[3] Reich S, Maultzsch J, Thomsen C and Ordejón P 2002 Tight-binding description of graphene *Phys. Rev.* B **66** 035412
[4] La Magna A, Deretzis I, Forte G and Pucci R 2008 Violation of the single-parameter scaling hypothesis in disordered graphene nanoribbons *Phys. Rev.* B **78** 153405
[5] Fiori G and Iannaccone G 2007 Simulation of graphene nanoribbon field-effect transistors *IEEE Electron Device Lett.* **28** 760–2
[6] Lin Y-M, Perebeinos V, Chen Z and Avouris P 2008 Electrical observation of subband formation in graphene nanoribbons *Phys. Rev.* B **78** 161409
[7] Liang G, Neophytou N, Lundstrom M S and Nikonov D E 2008 Contact effects in graphene nanoribbon transistors *Nano Lett.* **8** 1819–24
[8] Meyer J C, Kisielowski C, Erni R, Rossell M D, Crommie M F and Zettl A 2008 Direct imaging of lattice atoms and topological defects in graphene membranes *Nano Lett.* **8** 3582–6

[9] Wang X, Tabakman S M and Dai H 2008 Atomic layer deposition of metal oxides on pristine and functionalized graphene *J. Am. Chem. Soc.* **130** 8152–3

[10] Boukhvalov D W and Katsnelson M I 2008 Chemical functionalization of graphene with defects *Nano Lett.* **8** 4373–9

[11] Son Y-W, Cohen M L and Louie S G 2006 Energy gaps in graphene nanoribbons *Phys. Rev. Lett.* **97** 216803

[12] Huang B, Liu F, Wu J, Gu B-L and Duan W 2008 Suppression of spin polarization in graphene nanoribbons by edge defects and impurities *Phys. Rev.* B **77** 153411

[13] Strain M C, Scuseria G E and Frisch M J 1996 Achieving linear scaling for the electronic quantum coulomb problem *Science* **271** 51–3

[14] Izmaylov A F, Scuseria G E and Frisch M J 2006 Efficient evaluation of short-range Hartree-Fock exchange in large molecules and periodic systems *J. Chem. Phys.* **125** 104103

[15] White C, Johnson B G, Gill P M W and Head-Gordon M 1996 Linear scaling density functional calculations via the continuous fast multipole method *Chem. Phys. Lett.* **253** 268–78

[16] Scuseria G E 1999 Linear scaling density functional calculations with Gaussian orbitals *J. Phys. Chem.* A **103** 4782–90

[17] Fawcett J K and Trotter J 1966 The crystal and molecular structure of coronene *R. Soc. Lond. Proc. Ser.* A **289** 366–76

[18] Forte G, Grassi A, Lombardo G M, La Magna A, Angilella G G N, Pucci R and Vilardi R 2008 Modeling vacancies and hydrogen impurities in graphene: a molecular point of view *Phys. Lett.* A **372** 6168–74

[19] Hoffmann R 1963 An extended Hückel theory. I. Hydrocarbons *J. Chem. Phys.* **39** 1397–412

[20] Binkley J S, Pople J A and Hehre W J 1980 Self-consistent molecular orbital methods. 21. Small split-valence basis sets for first-row elements *J. Am. Chem. Soc.* **102** 939–47

[21] Gordon M S, Binkley J S, Pople J A, Pietro W J and Hehre W J 1982 Self-consistent molecular-orbital methods. 22. Small split-valence basis sets for second-row elements *J. Am. Chem. Soc.* **104** 2797–803

[22] Pietro W J, Francl M M, Hehre W J, DeFrees D J, Pople J A and Binkley J S 1982 Self-consistent molecular orbital methods. 24. Supplemented small split-valence basis sets for second-row elements *J. Am. Chem. Soc.* **104** 5039–48

[23] Hehre W J, Stewart R F and Pople J A 1969 Self-consistent molecular-orbital methods. I. Use of Gaussian expansions of slater-type atomic orbitals *J. Chem. Phys.* **51** 2657–64

[24] Collins J B, Schleyer P von R, Stephen Binkley J and Pople J A 1976 Self-consistent molecular orbital methods. XVII. Geometries and binding energies of second-row molecules. a comparison of three basis sets *J. Chem. Phys.* **64** 5142–51

[25] Frisch M J *et al* 2004 *Gaussian 03, Revision C.02* (Wallingford, CT: Gaussian, Inc.)

[26] Lee C, Yang W and Parr R G 1988 Development of the colle-salvetti correlation-energy formula into a functional of the electron density *Phys. Rev.* B **37** 785–9

[27] Becke A D 1993 Density-functional thermochemistry. III. The role of exact exchange *J. Chem. Phys.* **98** 5648–52

[28] Vosko S H, Wilk L and Nusair M 1980 Accurate spin-dependent electron liquid correlation energies for local spin density calculations: a critical analysis *Canad. J. Phys.* **58** 1200

[29] Stephens P J, Devlin F J, Chabalowski C F and Frisch M J 1994 *Ab initio* calculation of vibrational absorption and circular dichroism spectra using density functional force fields *J. Phys. Chem.* **98** 11623–7

[30] Modelli A, Mussoni L and Fabbri D 2006 Electron affinities of polycyclic aromatic hydrocarbons by means of b3lyp/6-31 + $g^*$ calculations *J. Phys. Chem.* A **110** 6482–6

[31] Bouzzine S M, Bouzakraoui S, Bouachrine M and Hamidi M 2005 Density functional theory (b3lyp/6-31$g^*$) study of oligothiophenes in their aromatic and polaronic states *J. Mol. Struct.-THEOCHEM* **726** 271–6

[32] Zahid F, Paulsson M and Datta S 2003 Electrical conduction through molecules *Advanced Semiconductors and Organic Nano-Techniques* ed M Morkoc (New York: Academic)

[33] Deretzis I and La Magna A 2006 Role of contact bonding on electronic transport in metal-carbon nanotube-metal systems *Nanotechnology* **17** 5063–72

[34] http://www.icmm.csic.es/jcerda/

[35] Kienle D, Cerda J I and Ghosh A W 2006 Extended Hückel theory for band structure, chemistry, and transport. I. Carbon nanotubes *J. Appl. Phys.* **100** 043714

[36] Cerdá J and Soria F 2000 Accurate and transferable extended Hückel-type tight-binding parameters *Phys. Rev.* B **61** 7965–71

[37] Datta S 2000 Nanoscale device modeling: the Green's function method *Superlatt. Microstruct.* **28** 253–78

[38] Schroeder P G, France C B, Parkinson B A and Schlaf R 2002 Orbital alignment at p-sexiphenyl and coronene/layered materials interfaces measured with photoemission spectroscopy *J. Appl. Phys.* **91** 9095–107

[39] Cho K A, Shimada T, Sakurai M and Koma A 1998 Effect of growth temperature and substrate materials on epitaxial growth of coronene *J. Appl. Phys.* **84** 268–74

[40] Zimmermann U and Karl N 1992 Epitaxial growth of coronene and hexa-peri-benzocoronene on mos2(0001) and graphite (0001): a LEED study of molecular size effects *Surf. Sci.* **268** 296–306

[41] Hill I G, Kahn A, Soos Z G and Pascal R A Jr 2000 Charge-separation energy in films of [pi]-conjugated organic molecules *Chem. Phys. Lett.* **327** 181–8

[42] Pereira V M, Lopes dos Santos J M B and Castro Neto A H 2008 Modeling disorder in graphene *Phys. Rev.* B **77** 115109

[43] Fujita M, Wakabayashi K, Nakada K and Kusakabe K 1996 Peculiar localized state at zigzag graphite edge *J. Phys. Soc. Japan* **65** 1920

[44] Fernández-Rossier J and Palacios J J 2007 Magnetism in graphene nanoislands *Phys. Rev. Lett.* **99** 177204

[45] Biel B, Triozon F, Blase X and Roche S 2009 Chemically induced mobility gaps in graphene nanoribbons: a route for upscaling device performances *Nano Lett.* **9** 2725–9

[46] La Magna A, Deretzis I, Forte G and Pucci R 2009 Conductance distribution in doped and defected graphene nanoribbons *Phys. Rev.* B **80** 195413

[47] Compagnini G, Giannazzo F, Sonde S, Raineri V and Rimini E 2009 Ion irradiation and defect formation in single layer graphene *Carbon* **47** 3201–7